Nat. Hazards Earth Syst. Sci. Discuss., 3, 2191–2219, 2015
www.nat-hazards-earth-syst-sci-discuss.net/3/2191/2015/
doi:10.5194/nhessd-3-2191-2015

Natural Hazards and Earth System Sciences
Open Access
Discussions

An assessment of the potential of earth observation data to detect and monitor storm cells associated with natural hazards – an application to an extreme weather event in southeastern Mediterranean

T. Mavrakou and C. Cartalis

Division of Physics, Department of Environmental Physics, University of Athens, 15874 Athens, Greece

Received: 2 February 2015 – Accepted: 22 February 2015 – Published: 1 April 2015

Correspondence to: T. Mavrakou (thmavrakou@phys.uoa.gr)

Published by Copernicus Publications on behalf of the European Geosciences Union.

Abstract

Storm cells that evolve in Mesoscale Convective Systems (MCSs) can be recognised with the use of satellite images. In this study, Meteosat images are used for the early detection and monitoring of the evolution of storm cells associated with MCSs. The developed methodology is based on the estimation of the "Airmass" and "Convective storm" composites, at fifteen minutes intervals. The methodology was applied on a selected four-day case study in February 2013, when a depression was developed over Africa and moved across the Mediterranean resulting in deep convection along its trajectory and in an extreme weather event (heavy rainfall associated with severe flooding) at the wider urban agglomeration of Athens. The produced composites detect potential vorticity (PV) anomaly related to cyclogenesis and increase the potential to detect and monitor storm cells associated with natural hazards.

1 Introduction

Satellite remote sensing may effectively detect and monitor Mesoscale Convective Systems (MCSs) thus as well as support the nowcasting of convective systems.

A Mesoscale Convective System (MCS) accounts for the occurrence of severe storm causing flooding and destructions (Houze, 2004). A MCS is a convective cloud and precipitation system quite larger than an individual storm and is characterized by extensive cloudiness in the middle and upper troposphere for hundred kilometres in the horizontal dimension (Glickman, 2000). It is developed from individual cells that interact with each other, merge and subsequently form a well-organized, long lived convective system (Cotton and Anthes, 1989). Houze (2004) points out that the dynamical processes of a MCSs are often more complex than those of individual cumulonimbus clouds, because when these clouds group together additional phenomena appear, like mesoscale circulations.

NHESSD

3, 2191–2219, 2015

According to a number of studies (Maddox, 1983; Cotton and Anthes, 1989; Anderson and Arritt, 1998; Laing and Fritsch, 2000), the causes for the development of MCSs are:

- existence of warm advection in the lower troposphere; the associated convection contributes to the development and the maintenance of an MCS;
- existence of strong south wind (low-level jet) with subsequent transfer of warm and moist air in the region of the MCS development;
- strong divergence in the region resulting in the enhancement of convection;
- convergence at the surface, often due to the existence of frontal surface.

In addition it was found that MCSs usually develop at the right entrance or left exit of jet stream.

Many researchers have attempted to predict and analyse deep convection, thus possible MCS development (Pankiewicz, 1997; Vila and Machado, 2004; Kolios and Feidas, 2010). Melani et al. (2013) highlights the key role of the Mediterranean Sea in the development of the MCSs and points out the significance of the mechanism of convective initiation for the forecasting improvement. Furthermore, Pajek et al. (2007) indicate that "the process of storm development consists of pre-storm conditions leading to the development of convection followed by development of deep convective clouds, which became storm cells after the first lightining"; they also concluded that the use of satellite data at specific spectral channels may increase lead-time for storm nowcasting.

Pre-storm conditions are characterized by instability in the atmosphere which results in deep convection and consequently to the development of storm cells (Pajek et al., 2007). Atmospheric instability during winter, over southeast Europe, is generated when cold continental air mass encounters a warmer Mediterranean one. Evaporation that takes place over the relative warm Mediterranean and Greek maritime areas enforces this instability, while during the cold period of the year Greece is affected mainly

NHESSD
3, 2191–2219, 2015

by westward depressions formed over the Mediterranean (Cartalis et al., 2004). According to some authors (Petterssen, 1956; Radinovic, 1987; Campins et al., 2000) the Mediterranean region is one of the most cyclogenetic regions in the world, while the Mediterranean cyclone structure can be well described with the use of the midlatitude conveyor belt model (Ziv et al., 2010) and the cyclogenetic mechanism has been well explained through the potential vorticity (PV) dynamics (Hoskins et al., 1985; Davis and Emanuel, 1991). Therefore, black lines in the water vapour satellite images are associated with the inflow of dry stratospheric air and consequently could serve as indicators of imminent cyclogenetic events (Michel and Bouttier, 2006). An example of a Meteosat water vapour image depicting dry air intrusion in a Mediterranean cyclone is illustrated in a study regarding the relation of midlatitude conveyor belts to winter Mediterranean cyclones (Ziv et al., 2010).

Regarding the eastern Mediterranean and specifically Greece, Feidas et al. (2000) developed a cloud classification scheme of satellite images in the visible, infrared and water vapour channels aiming to define and monitor heavy rain associated cloud cells. Feidas and Cartalis (2001) developed an automated algorithm, capable of locating regions that are characterized by deep convection and consequently of detecting and monitoring MCSs until the point of dissipation. The algorithm was applied to events characterized by heavy rainfall in Greece; it detected several MCSs on infrared and water vapour satellite images (Feidas and Cartalis, 2001, 2005). However, the above techniques employed Meteosat First Generation (MFG) satellite data of lower temporal, spatial and spectral resolutions as compared to Meteosat Second Generation (MSG).

The MSG satellite provides data which, apart from the better spatial and temporal resolutions, is of improved spectral resolution thus enabling the application of multispectral techniques in many fields such as surface observations, fire and cloud detection, etc. (Casanova et al., 2010). Giannakos and Feidas (2013) used brightness temperature differences as spectral parameters, along with textural differences as derived from the infrared MSG channel, in order to classify stratiform and convective rain. In addition, the technique described by Negri et al. (2014) assumes that combinations

NHESSD
3, 2191–2219, 2015

of infrared pairsof the SEVIRI channel allow the isolation of specific cloud components (droplets or ice particles with different shape and size) and then the tracking of the displacement of these structures, so as to detect deep convection cloud-tops.

Furthermore, composites enable the visualisation of multispectral physical features in a single image, such as pre-storm conditions and storm cell characteristics. The MSG composites proposed by Kerkmann et al. (2006) have been used in studies for the detection and analysis of MCSs in Europe (Pajek et al., 2007; Feidas, 2012). In an operational approach towards the nowcasting of an MCS development in south-west Italy, Gallino and Turato (2007) presented the importance of the 6.2 µm spectral channel as it depicts in detail the conditions in the upper troposphere which have an important role in the development of the MCSs. At the same time they suggested the use of the Convective storm composite in MCS detection so as to support the the distinction of young and severe storms in daytime. Among other differences this composite employs the 3.9–10.8 µm channel difference resulting in the depiction of small ice particles, which reflects a feature of deep convection and severe weather. In another study, regarding two MCSs that crossed Hungary in 2006, Putsay et al. (2009) used the Airmass composite for the interpretation of the synoptic conditions during day and night. This composite allows the distinction of different air masses, of the cloudiness linked with frontal surfaces and of the jet stream, i.e. factors that affect instability and consequently the development of a MCS.

In this study a standalone algorithm for the production of composites is developed and applied for an extreme weather event which occurred in the region of Athens in February 2013. All composites are produced at fifteen minutes intervals in an effort to track MCSs from the time of genesis until the time of dissipation. The potential of the algorithm to support operational nowcasting is examined, in relation also to ground based measurements of precipitation.

NHESSD
3, 2191–2219, 2015

2 Data

The area of study is provided in Fig. 1 in Meteosat projection; it covers Central Europe and the Eastern Mediterranean (59°04′00″ N, 06°97′00″ W, 28°23′00″ N, 30°00′00″ E). The study is further concentrated to the Attica region and the wider urban agglomeration of Athens.

Meteosat 8 images, for five infrared and two visible channels, were obtained for the period 19–22 February 2013. The Airmass and Convective storm composites were produced at fifteen minute intervals using the channels shown in Table 1. In addition, synoptic charts were used covering the same area and time period, in order to verify the results as well as to support their analysis. Precipitation data, at ten minutes intervals, were collected from eight stations (network of the National and Technical University of Athens) within the Attica region (Fig. 2).

3 Methodology

The methodology for the early detection of storm cells consists of the following steps:

- development of an algorithm for Airmass and Convective storm composites production; the Airmass and Convective storm composites are considered appropriate for the depiction of the pre-storm conditions and the analysis of the associated severe weather, whereas their combination allows the continuous monitoring of their evolution in time;
- application of the composites for a case study reflecting an extreme weather event;
- evaluate the potential of the methodology for the detection of MCS and the subsequent improvement of operational nowcasting.

The Airmass composite provides data in day and night as it consists of two water vapour channels with centre wavelengths at 6.2 (WV6.2) and 7.3 µm (WV7.3) and two

NHESSD
3, 2191–2219, 2015

infrared channels with centre wavelengths at 9.7 (IR9.7) and 10.8 µm (IR10.8) in the following combination:

RED = WV6.2 – WV7.3

GREEN = IR9.7 – IR10.8

BLUE = WV6.2.

The Convective storm composite provides data in daytime only as it consists of four infrared channels with wavelengths at 6.2 (WV6.2), 7.3 (WV7.3), 3.9 (IR3.9), 10.8 µm (IR10.8) and one visible channel with wavelengths at 0.6 (VIS0.6) and one in the near infrared at 1.6 µm (NIR1,6) in the following combination:

RED = WV6.2 – WV7.3

GREEN = IR3.9 – IR10.8

BLUE = NIR1.6 – VIS0.6.

The Airmass composite was selected in order to define potential instability in the atmosphere (and in particular to monitor synoptic conditions, upper level dynamics and different air masses). The Convective storm composite was selected so as to monitor the convection related to storm development, i.e. strong updrafts as depicted through the detection of small ice particles in the upper troposphere.

During night time, and due to lack of data in the visible bands, the Convective storm composite is not applicable and the use of Airmass composite is extended for the detection of storm cells. This is accomplished by adapting the traditional approach of storm cell detection in the Airmass composite interpretation. According to Feidas and Cartalis (2001), a storm cell is defined as a cloud system with low brightness temperature in the IR channels with specific geometrical characteristics (circular).

NHESSD

3, 2191–2219, 2015

Processing the satellite data

The procedure followed for the production of the Airmass and the Convective storm composites is analysed below while the overall procedure for both composites is presented also as a flow chart in Figs. 3 and 4 respectively.

The developed Airmass algorithm (Fig. 3) converts pixel values to brightness temperature, calculates the brightness temperature differences and applies Gamma correction and colour to the resulted differences. The difference in the red channel provides information about the altitude of a humid layer or cloud as the two WV channels detect humidity in different altitudes. The difference in green provides information about the ozone concentration in the atmosphere and consequently about the height of the tropopause, the existence of warm or cold air masses and the intrusion of ozone-rich stratospheric air. Furthermore, in blue the WV6.2 channel is assigned, giving information on the existence of humidity or cloudiness in the layer 500–200 hPa. In the Airmass image, the above physical features are preserved through the assignment of the scale in the Brightness Temperature Differences (BTD) values. Green colours indicate warm air masses, while blue shades indicate cold air masses. White colour corresponds to height precipitating clouds while whiter and brighter colours indicate high altitude clouds and consequently low temperatures. Red colours indicate dry stratospheric air and consequently enabling monitoring the jet stream.

The developed Convective storm algorithm (Fig. 4) processes infrared data in a similar way as the Airmass one. Additionally, it calculates the BT 3.9 CO_2 correction, as this channel lies close to the CO_2 absorption band, and it calculates the solar zenith angle per pixel. It should be mentioned that the latter is essential for the calculation of reflectance in the bands in the visible. The difference in the red has been discussed above (see Airmass composite). Regarding green, the 3.9 µm radiance consists of a solar and a thermal component during daytime, while reflection at this wavelength is sensitive to cloud phase and very sensitive to particle size (high reflection indicates small particles). Consequently, by subtracting the 10.8 µm channel, the resulting val-

NHESSD
3, 2191–2219, 2015

ues indicate water or ice clouds with small or large particles. The difference between NIR1.6 and VIS0.6 in blue provides information about the phase of the particles as the absorption at 1.6 µm is highest for the ice than for the water particles. The Convective storm image illustrates deep convection, strong updrafts with small ice particles, from orange to yellow colours depending on the strength of the updraft, while pink colour depicts precipitating clouds. Blue shades illustrate land and ocean.

In this study, improvements of the algorithms refer to (a) the estimation of the solar zenith angle per pixel, thus enabling the processing of MSG data, and (b) the production of the composites every 15 min.

4 Case study results and analysis

4.1 The period from 19 to 21 February 2013

The Airmass and Convective storm composites were produced for four consecutive days 19, 20, 21, 22 February 2013, i.e. at a time period when a low pressure system was developed over northwest Africa, moved eastward towards Greece causing instability and convection over the regions which lie along the trajectory of the system.

During 19 February, stratospheric dry air was detected over the western part of Europe, specifically from Great Britain to northwest Africa as it can be seen from the reddish colour in the Airmass image at 12:00 UTC (Fig. 5a). At the same time, the 1 PVU level (Fig. 5b) over western Europe is at 500 hPa, which implies that stratospheric air has protruded to mid troposphere, as it has been detected for the same region also from the Airmass image (Fig. 5a).The stratospheric intrusion is connected with high potential vorticity values which in turn are related to cyclogenesis. Indeed, on 20 February at 00:00 UTC (Fig. 5c) a depression was formed over the northwest Africa, while at 12:00 UTC (Fig. 6a) the depression was further developed. The Airmass image (Fig. 6a) depicts clearly (with blue and green colours) the different air masses associated to the depression; the image thus depicts clearly the cold and warm sec-

NHESSD
3, 2191–2219, 2015

tors respectively. In addition, due to the satisfactory depiction of the cloud structure, the cold and warm fronts can be identified in the Airmass image (Fig. 6a) through the developed clouds within the depression.

The sequence of the Airmass images (Fig. 6) concerning the aforementioned days shows the trajectory of the depression. According to the trajectory, the depression followed a zonal track from the west towards the east. The depression moved along the African coast, beginning from northwest Africa on 20 February at 12:00 UTC (Fig. 6a), passing over Sicily on 21 February at 12:00 UTC (Fig. 6b and c) and located over south Greece on the 22 February at 00:00 UTC (Fig. 6d). This is a typical trajectory (easterly track) of African depressions in February that differs from the respective trajectory in December and January. The latter has a north component resulting in a northeast movement of the depression, thus affecting western Mediterranean (Alpert et al., 1990).

Synoptic analysis for these days is presented on Fig. 7. Subsequent to the aforementioned PV anomaly, a depression was developed on 20 February at 00:00 UTC, located over northwest Africa with 1001 hPa centre pressure (Fig. 7a), accompanied by a cut-off low in the upper troposphere (Fig. 7b). Furthermore, on 22 February, the warm sector of the depression is located over Greece (Fig. 7c), while its centre lies easterly. The 500 hPa height analysis (Fig. 7d) shows an extended trough located over central Europe and a disturbance connected with the surface depression located over the Ionian Sea. It should be mentioned that the aforementioned synoptic situation is similar to an examined one by Feidas et al. (2004) which was classified as a west Depressional Weather Type in the classification of cold period weather types in Greece. It is found that this type is related with convective activity and atmospheric instability.

The passage of the depression over south Italy and Greece caused instability and resulted in the development of convective cells over Sicily and Attica respectively. The Convective storm images, as presented in sequence every fifteen minutes (Fig. 8), contribute to the recognition, the diagnosis and the monitoring of the storm cells and their evolution to MCSs. In the event, that the time scale was of the order of sixty minutes, the potential of the methodology would have been reduced.

NHESSD
3, 2191–2219, 2015

On 21 February after 12:57 UTC, the Convective image (Fig. 8a–e) detects convective cells (circular shape with orange to yellow colours) over Sicily. Subsequently, after 14:12 UTC the merging of the storm cells which have evolved in MCSs is clearly observed (Fig. 8f). Both MCSs continue to be yellow and to grow in size (Fig. 8g–i) indicating deep convection without reaching yet the mature stages of their lifecycle. Furthermore, after 15:12 UTC (Fig. 8j–l) the convective cells appear in pink signifying the weakening of the updraft or the weakness of the Convective storm composite to provide reliable information due to the solar zenith angle that approaches high values at sunset.

During the night of 22 February, convective cells were developed over Attica, while in the morning hours, and due to merging of the storm cells, a large Mesoscale Convective System (MCS) is recognized (orange colour) in the Convective image at 09:42 UTC (Fig. 9a). The MCS continues to grow in size without further affecting Attica, as it moves toward southeast, (Fig. 9b–f) while at 11:12 UTC (Fig. 9g) new cells develop (bright yellow colour) within the southeast part of the MCS, highlighting the supply of the MCS with warm and moist air from the southeast, a fact which indicates that the MCS has not yet reached the stage of dissipation (Fig. 9h–l). Furthermore, convective activity is observed near the MCS for the entire duration of its evolution. Consequently, the application of the Convective composite to the above weather event shows its usefulness for the monitoring analysis of the evolution of a MCS and thus demonstrates its capacity to support nowcasting.

4.2 22 February 2013

During the night of 22 February a series of extreme weather events occurred over Attica and were related to the development of storm cells. At 00:00 UTC the warm sector of the low pressure system was located over Greece (Fig. 7c). The south surface wind was supplying Attica with warm and moist air, while at 850 hPa the same region was characterized by warm advection and southeasterly winds. The passing of the cold front coupled with the aforementioned situation led to the development of deep

NHESSD
3, 2191–2219, 2015

convection over Attica after 01:57 UTC. It should be mentioned that the total amount of precipitation for the eight hours period (02:00 to 10:00 UTC) for all stations within Attica (Fig. 10), reflects the severity of the events. For instance, Zografou station recorded 103 mm, while the mean monthly precipitation for February in Attica is 55–65 mm.

The use of Airmass composite (Fig. 11a–d) in conjunction with precipitation data every ten minutes (Fig. 12) at the three stations that are located at the west, at the centre and at the east of Attica, respectively, demonstrates the usefulness of this composite in nowcasting.

The first storm cell that was developed due to synoptic factors, is depicted in Airmass composite at 01:57 UTC (Fig. 11a), i.e. forty to fifty minutes before the extreme weather event's first maximum (Fig. 12). Subsequently, this storm cell evolved in a backward MCS and the cold air as trapped in the Athens basin from the first MCS, and combined with the south winds, established the conditions for further MCS development.

The second and the third storm cells are depicted at 02:57 UTC (Fig. 11b) and at 05:40 UTC (Fig. 11c), respectively. These MCSs were depicted more than one hour earlier of the event, third and fourth maxima (Fig. 12) and eventually both of them evolved in forward MCSs. Finally, the merging of the two MCSs is depicted at 06:57 UTC (Fig. 11d), twenty minutes earlier of the event and resulted in the reinforcement of the extreme event for the fourth time (Fig. 12).

Finally, the differences in the precipitation distribution between the three stations are attributed to the change in direction of the mean wind in 850–300 hPa layer. After their development within the MCS, the cells moved downwind with the mean wind affecting different regions depending on the wind direction. Particularly, the cells of the first MCS moved towards north, as the mean wind was south, affecting Ano Liosia and Galatsi stations. Subsequently the south mean wind started to have a west component and carried the cells towards northeast of Attica (Zografou station).

NHESSD
3, 2191–2219, 2015

5 Conclusion

This research study aims at demonstrating the potential for the early detection and adequate monitoring of storm cells associated to natural hazards. The developed methodology was applied for a four day long case study in February 2013, when a low pressure system developed over Africa and moved north eastward towards Greece causing instability along its trajectory. The methodology focuses in particular to the series of extreme weather events that occurred on the 22 February 2013 for a period of seven hours over Attica.

The standalone algorithm that was developed for the production of the composites (Airmass and Convective storm), provides all products at fifteen minutes interval, a fact which improves the capacity to operationally observe the evolution of a MCS as well as it merging to other MCSs. The application of these composites shows that the Airmass composite depicts well the synoptic situation and detects the PV anomaly prior to the depression development. The extended use of this composite to storm cell detection, allowed the detection of three MCS that produced four precipitation maxima. Comparing the distribution of the precipitation amount with the produced images, it is deduced that the methodology enables the detection of three storm cells at least one hour earlier from the events in all stations and twenty minutes earlier from the merging of the cells. Furthermore, the application of the Convective storm, when available, to the above weather event shows its usefulness for the monitoring of the evolution of MCS. In particular, the use of the Convective storim allowed the depiction of deep convection over Sicily and Attica, as well as the identification of the MCS region where the new cells developed.

In conclusion, despite the limitations (for instance the lack of the Convenctive Storm composite during night time), the performed analysis demonstrate the potential of earth observation, once combined with ground based data, for the recognition, the analysis and the monitoring of the MCSs associated with natural hazards. Taken the potential impacts of natural hazards to human well being, a critical prerequisite for the monitor-

NHESSD
3, 2191–2219, 2015

ing of the MCSs is the rapid re-examination of the prevailing meteorological and storm cell conditions; such prerequisite is satisfied by developing the Air Mass and Convective storm composites at fifteen minutes intervals. Finally further work is needed, for instance the use of additional composites to compensate for the lack of the Convective storm one at night, so as to improve the analysis and support nowcasting techniques.

References

Alpert, P., Neeman, B. U., and Shay-el, Y.: Intermonthly variability of cyclone tracks in the Mediterranean, J. Climate, 3, 1474–1478, 1990.

Anderson, C. J. and Arritt, R. W.: Mesoscale convective complexes and persistent elongated convective systems over the United States during 1992 and 1993, Mon. Weather Rev., 126, 578–599, 1998.

Campins, J., Genovés, A., Jansà, A., Guijarro, A. J., and Ramis, C.: A catalogue and a classification of surface cyclones for the western Mediterranean, Int. J. Climatol., 20, 969–984, 2000.

Cartalis, C., Chrysoulakis, N., Feidas, H., and Pitsitakis, N.: Categorization of cold period weather types in Greece on the basis of the photointerpretation of NOAA/AVHRR imagery, Int. J. Remote Sens., 25, 2951–2977, 2004.

Casanova, C., Romo, A., Hernández, E., and Casanova, L. J.: Operational cloud classification for the Iberian Peninsula using Meteosat Second Generation and AQUA-AIRS image fusion, Int. J. Remote Sens., 31, 93–115, 2010.

Cotton, W. R. and Anthes, R. A.: Storm and Cloud Dynamics, Academic Press, San Diego, 1989.

Davis, C. and Emanuel, K.: Potential vorticity diagnostics of cyclogenesis, Mon. Weather Rev., 119, 1929–1953, 1991.

Feidas, H.: Study of a mesoscale convective complex over Balkans with Meteosat data, in: Advances in Meteorology, Climatology and Atmospheric Physics, Springer Atmospheric Sciences, Springer, Berlin, Heidelberg, 79–85, 2012.

Feidas, H. and Cartalis, C.: Monitoring mesoscale convective cloud systems associated with heavy storms using meteosat imagery, J. Appl. Meteorol., 40, 491–512, 2001.

NHESSD
3, 2191–2219, 2015

Feidas, H. and Cartalis, C.: Application of an automated cloud-tracking algorithm on satellite imagery and monitoring small mesoscale convective cloud systems, Int. J. Remote Sens., 26, 1677–1698, 2005.
Feidas, H., Cartalis, C., and Cracknell, A.: Use of Meteosat imagery to define clouds linked with floods in Greece, Int. J. Remote Sens., 21, 1047–1072, 2000.
Gallino, S. and Turato, B.: An operational approach to the nowcasting of an intense thunderstorm over Liguria, Adv. Geosci., 7, 395–400, doi:10.5194/adgeo-7-395-2007, 2007.
Giannakos, A. and Feidas, H.: Classification of convective and stratiform rain based on the spectral and textural features of Meteosat Second Generation infrared data, Theor. Appl. Climatol., 113, 495–510, 2013.
Glickman, T.: Glossary of Meteorology, 2nd Edn., American Meteorological Society, Boston, 855 pp., 2000.
Hoskins, J. B., McIntyre, E. M., and Robertson, W. A.: On the use and significance of isentropic potential vorticity maps, Q. J. Roy. Meteorol. Soc., 111, 877–946, 1985.
Houze, R.: Mesoscale convective systems, Rev. Geophys., 42, RG4003, doi:10.1029/2004RG000150, 2004.
Kerkmann, J., Rosenfeld, D., Bridge, G., and Roesli, H.: RGB composites with channels 1–11 and their interpretation, available at: http://www.eumetrain.org/IntGuide/ (last access: 20 November 2014), 2006.
Kolios, S. and Feidas, H.: A warm season climatology of mesoscale convective systems in the Mediterranean basin using satellite data, Theor. Appl. Climatol., 102, 29–42, 2010.
Laing, A. G. and Fritsch, J. M.: The large-scale environments of the global populations of mesoscale convective complexes, Mon. Weather Rev., 128, 2756–2776, 2000.
Maddox, R. A.: Large-scale meteorological conditions associated with midlatitude, mesoscale convective complexes, Mon. Weather Rev., 111, 126–140, 1983.
Melani, S., Pasi, F., Gozzini, B., and Ortolani, A.: A four year (2007–2010) analysis of long-lasting deep convective systems in the Mediterranean basin, Atmos. Res., 123, 151–166, 2013.
Michel, Y. and Bouttier, F.: Automated tracking of dry intrusions on satellite water vapour imagery and model output, Q. J. Roy. Meteorol. Soc., 132, 2257–2276, 2006.
Negri, G. R., Machado, T. A. L., and Borde, R.: Inner convective system cloud-top wind estimation using multichannel infrared satellite images, Int. J. Remote Sens., 35, 651–670, 2014.

NHESSD
3, 2191–2219, 2015

Pajek, M., Iwanski, R., Konig, M., and Struzik, P.: Extreme Convective Cases – The use of Satellite Products for Storm Nowcasting and Monitoring, EUMETSAT Conference Report, Darmstadt, Germany, 2007.
Pankiewicz, S. G.: Neural network classification of convective airmasses for flood forecasting system, Int. J. Remote Sens., 18, 887–898, 1997.
Petterssen, S.: Weather Analysis and Forecasting, vol. 1, MacGraw-Hill, New York, 428 pp., 1956.
Putsay, M., Szenyan, I., and Simon, A.: Case study of mesoscale convective systems over Hungary on 29 June 2006 with satellite, radar and lightning data, Atmos. Res., 93, 82–92, 2009.
Radinovic, D.: Mediterranean cyclones and their influence on the weather and the climate, PSMP Rep. Ser. no. 24, WMO, 1987.
Vila, A. D. and Machado, T. A. L.: Shape and radiative properties of convective systems observed from infrared satellite images, Int. J. Remote Sens., 25, 4441–4456, 2004.
Ziv, B., Saaroni, H., Romem, M., Heifetz, E., Harnik, N., and Baharad, A.: Analysis of conveyor belts in winter Mediterranean cyclones, Theor. Appl. Climatol., 99, 441–455, 2010.

NHESSD
3, 2191–2219, 2015

Table 1. Characteristics of the eight MSG channels used for the composites production.

Channel No.	Spectral Band (μm)	Range of spectral band (μm)	Main observational application
01	VIS0.6	0.56–0.71	Surface, clouds, wind fields
03	NIR1.6	1.50–1.78	Surface, cloud phase
04	IR3.9	3.48–4.36	Surface, clouds, wind fields
05	WV6.2	5.35–7.15	Water vapor, high level clouds, atmospheric instability
06	WV7.3	6.85–7.85	Water vapor, atmospheric instability
08	IR9.7	9.38–9.94	Ozone
09	IR10.8	9.80–11.80	Surface, clouds, wind fields, atmospheric instability
11	IR13.4	12.40–14.40	Cirrus cloud height

NHESSD
3, 2191–2219, 2015

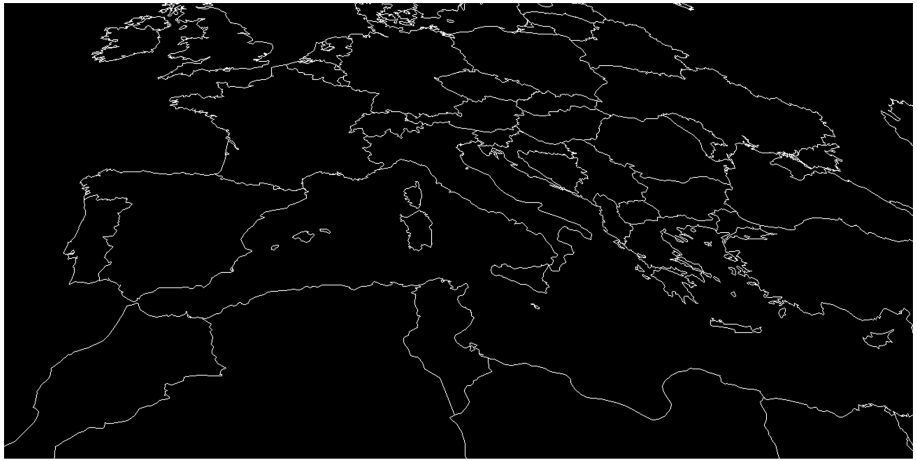

Figure 1. Area of study in Meteosat projection.

NHESSD
3, 2191–2219, 2015

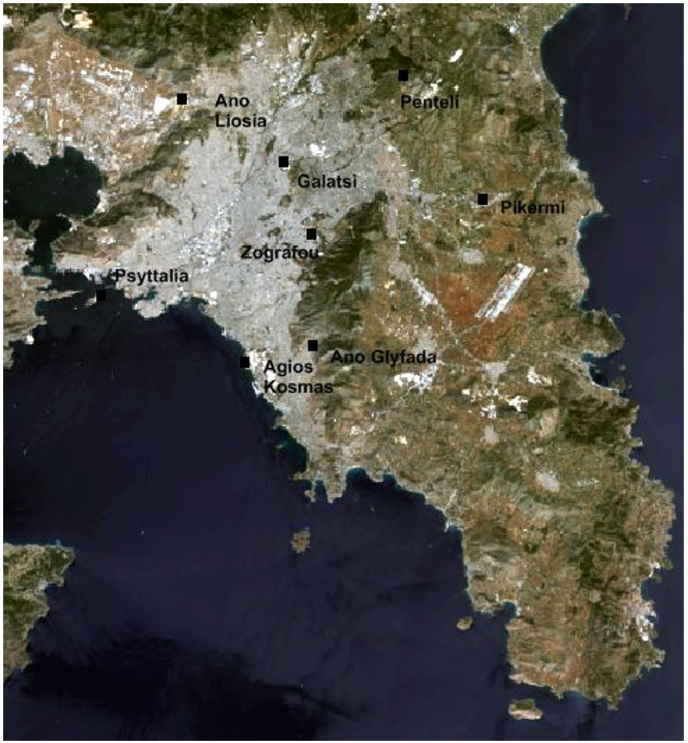

Figure 2. Attica region and the location of the eight meteorological stations.

NHESSD
3, 2191–2219, 2015

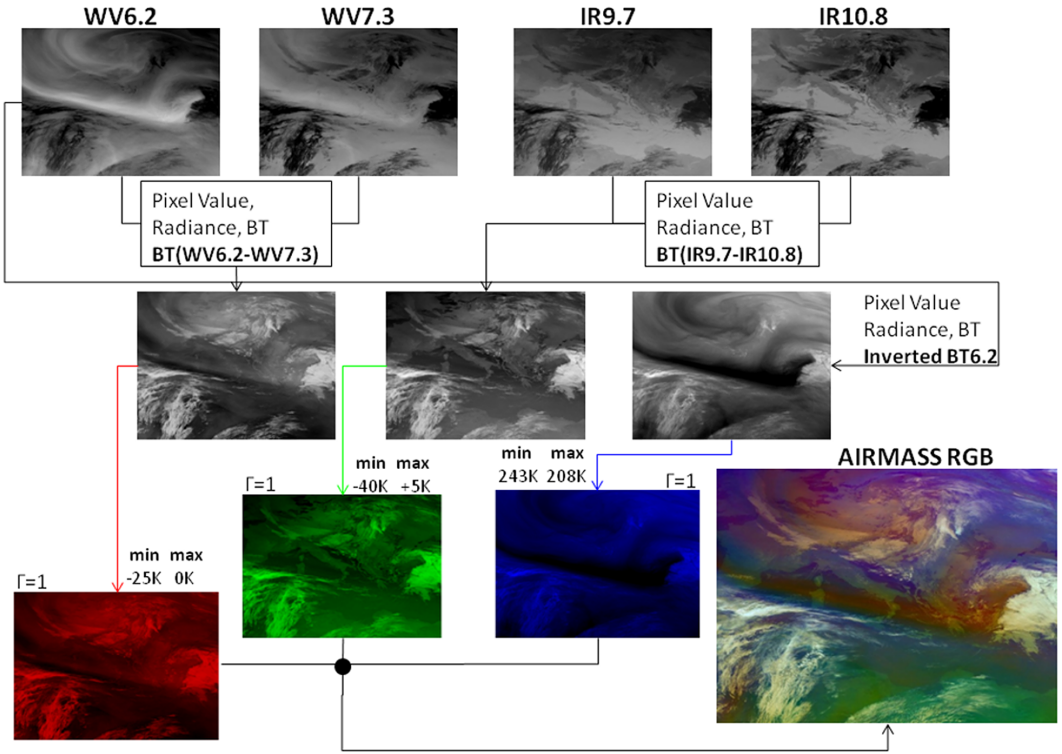

Figure 3. Flow chart of the Airmass algorithm.

NHESSD
3, 2191–2219, 2015

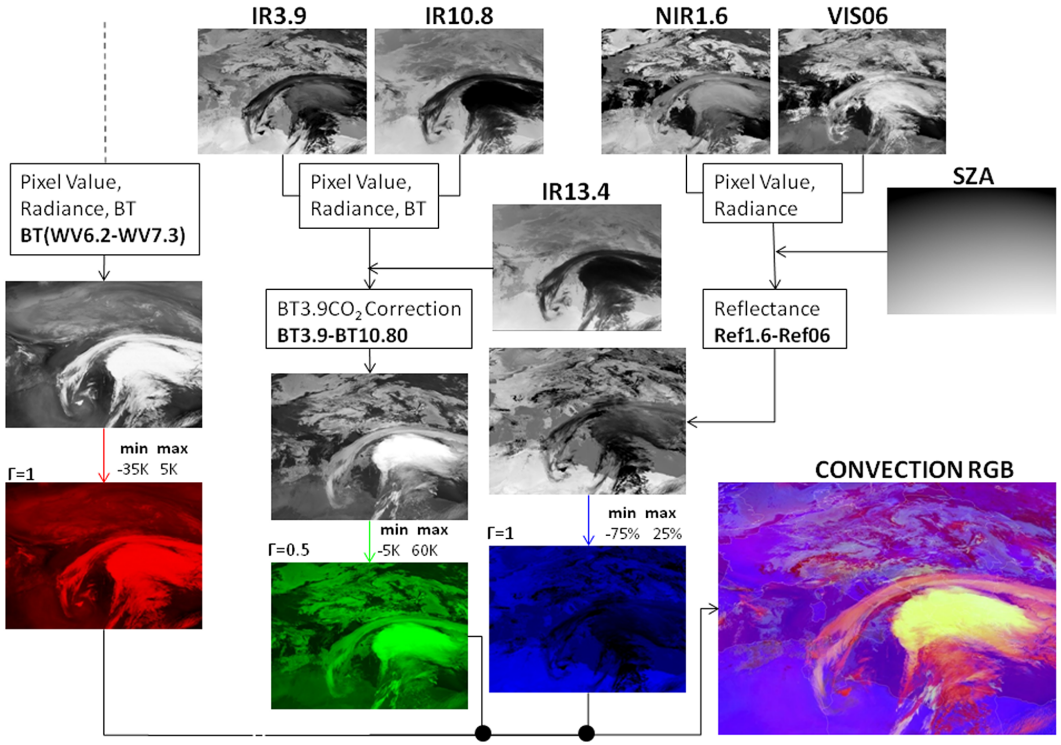

Figure 4. Flow chart of the Convection algorithm.

NHESSD
3, 2191–2219, 2015

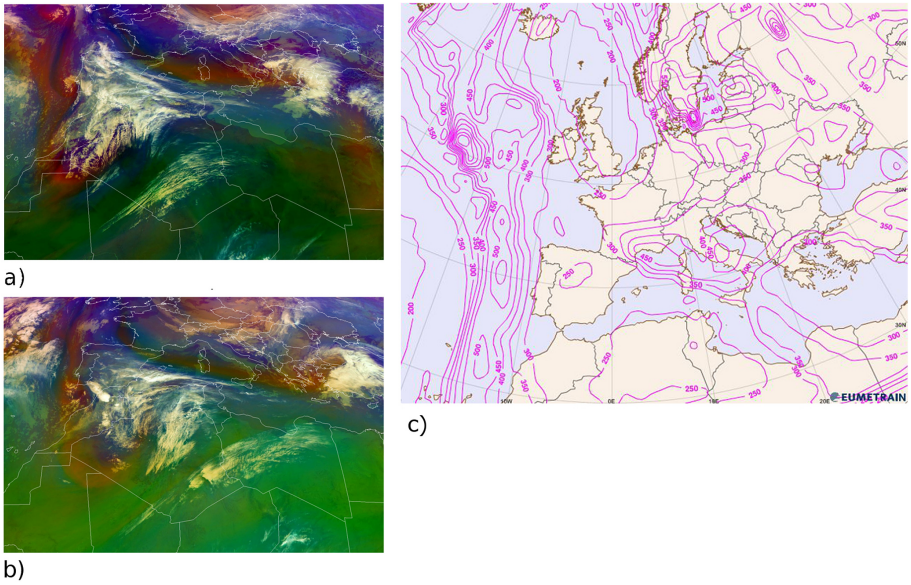

Figure 5. Airmass composite images on **(a)** 19 February at 12:00 UTC, **(b)** 20 February at 00:00 UTC and **(c)** 1 PVU level on 19 February at 12:00 UTC.

NHESSD
3, 2191–2219, 2015

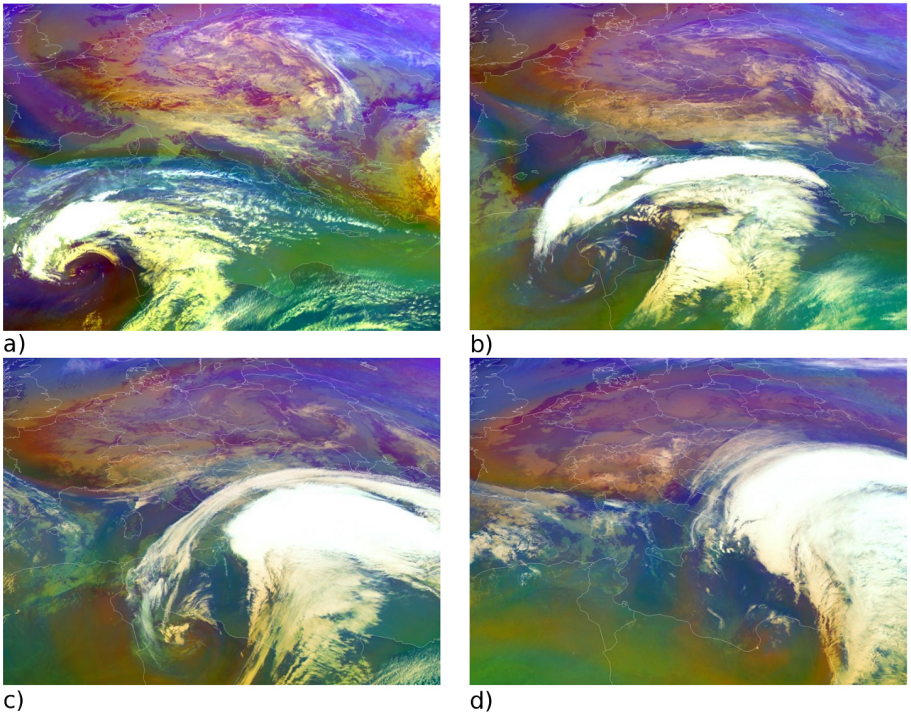

Figure 6. Sequence of Airmass images on **(a)** 20 February at 12:00 UTC, **(b)** 21 February at 00:00 UTC, **(c)** 21 February at 12:00 UTC and **(d)** 22 February at 00:00 UTC.

NHESSD
3, 2191–2219, 2015

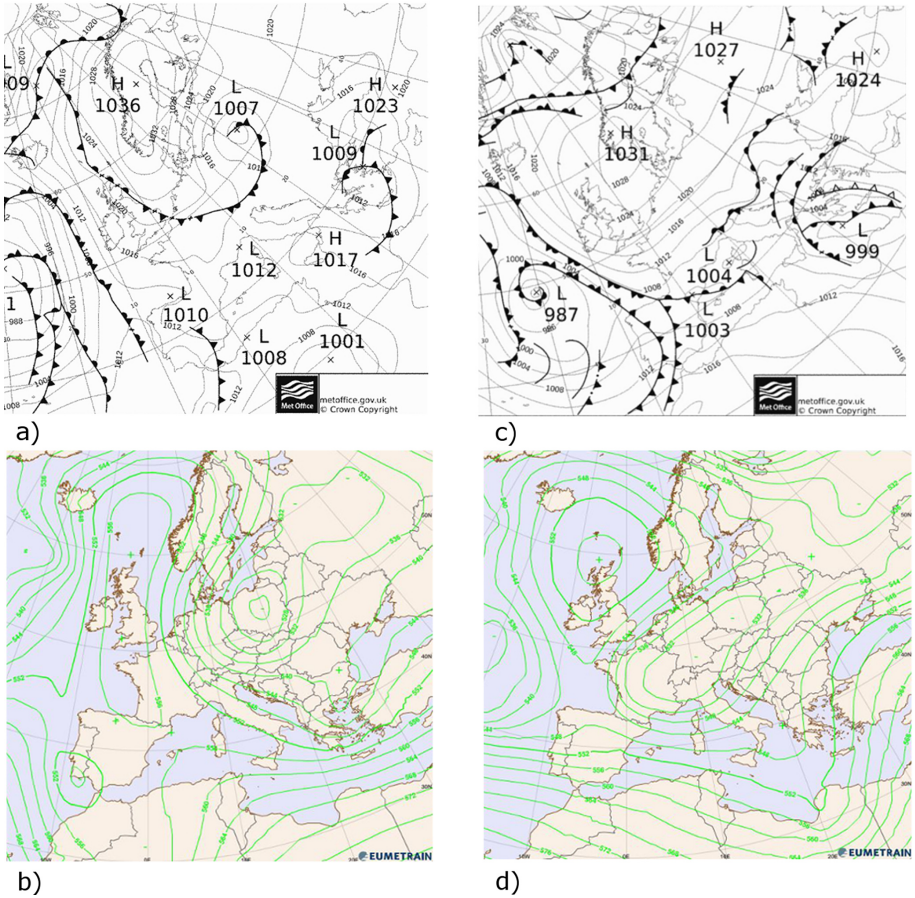

Figure 7. Synoptic charts for different atmospheric levels on 20 February at 00:00 UTC **(a)** surface pressure chart, **(b)** 500 hPa geopotential height and on 22 February at 12:00 UTC **(c)** surface pressure chart and **(d)** 500 hPa geopotential height.

NHESSD
3, 2191–2219, 2015

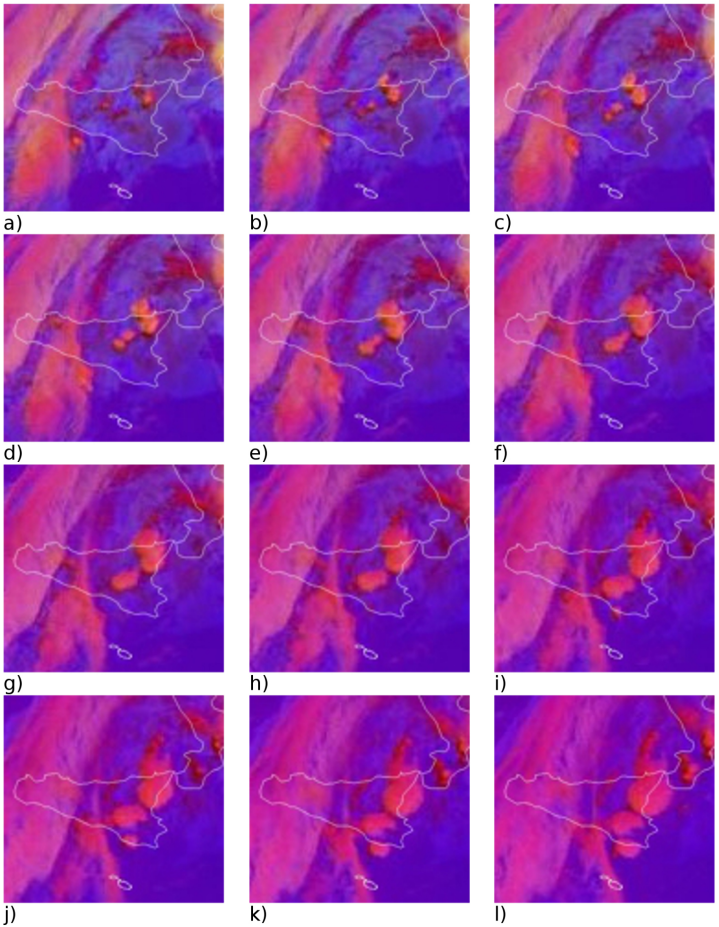

Figure 8. Convective storm images (focused on Sicily) on 21 February every fifteen minutes from **(a)** 12:57 to **(l)** 15:42 UTC.

NHESSD
3, 2191–2219, 2015

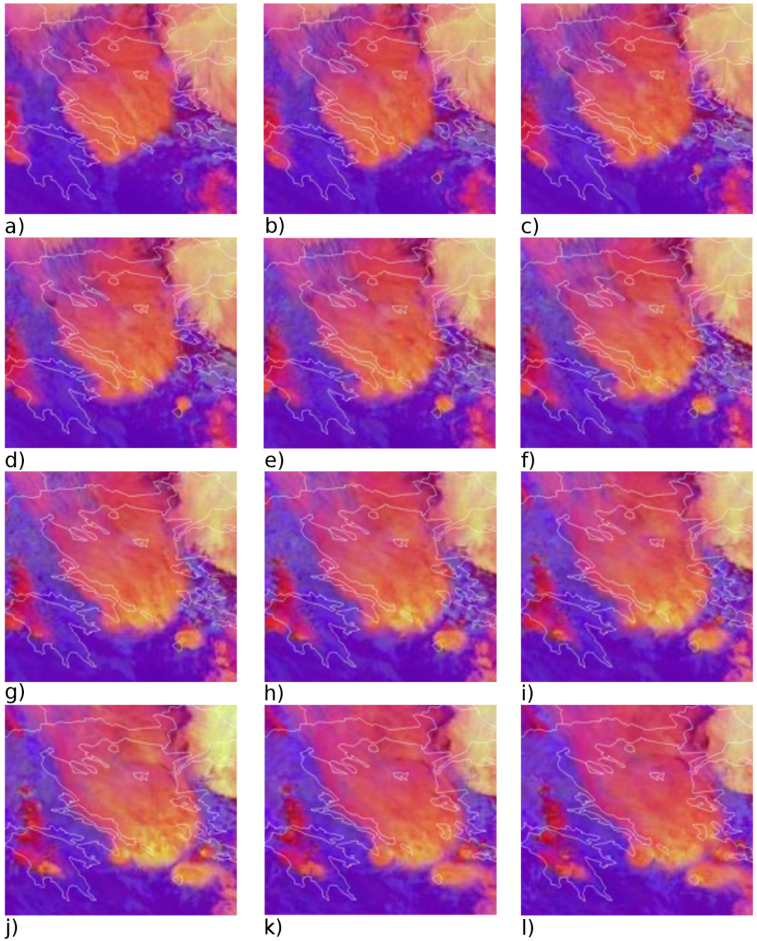

Figure 9. Convective storm composite images (focused on Attica) on 22 February every fifteen minutes from **(a)** 09:42 to **(l)** 12:27 UTC.

NHESSD
3, 2191–2219, 2015

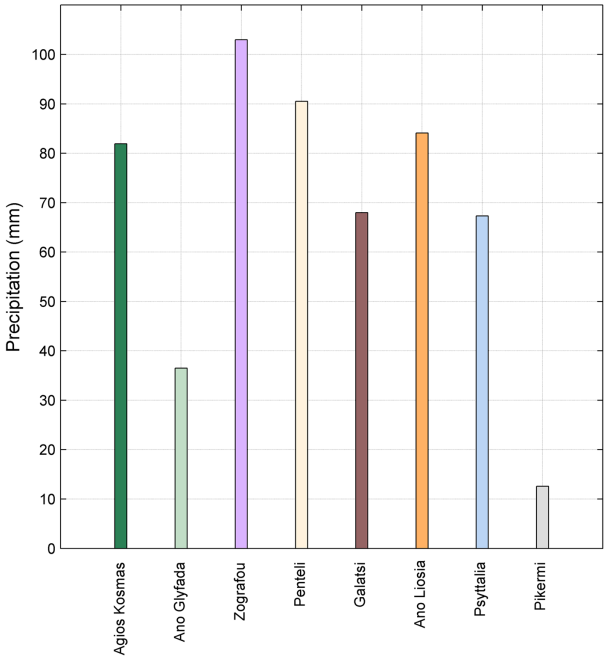

Figure 10. Total amount of precipitation for the eight hours period (02:00 to 10:00 UTC) for all stations within Attica.

NHESSD
3, 2191–2219, 2015

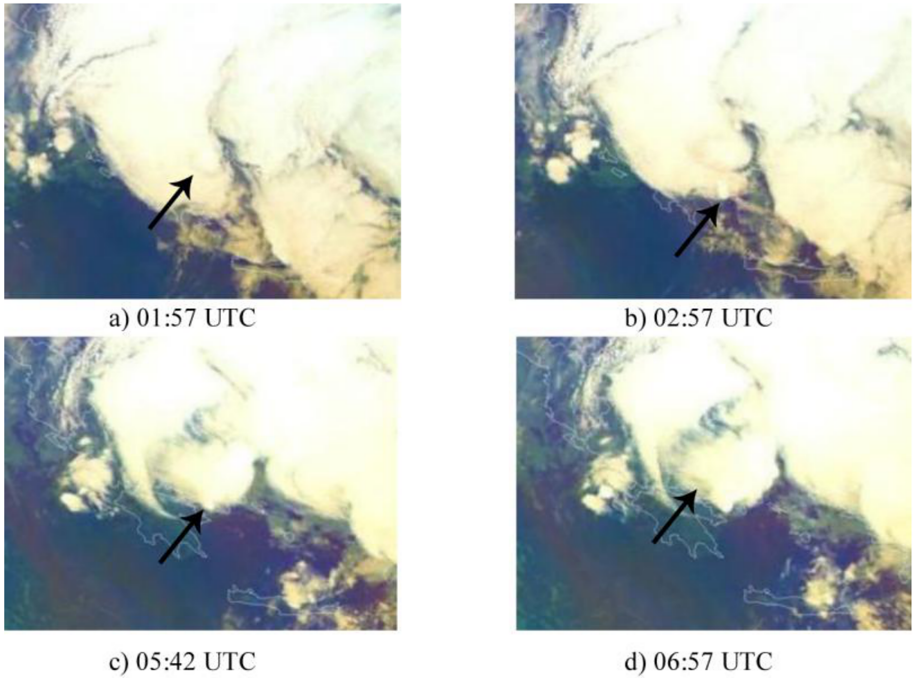

Figure 11. Airmass composite (focused on Attica) on 22 February at **(a)** 01:57, **(b)** 02:57, **(c)** 05:40 and **(d)** 06:57 UTC.

NHESSD
3, 2191–2219, 2015

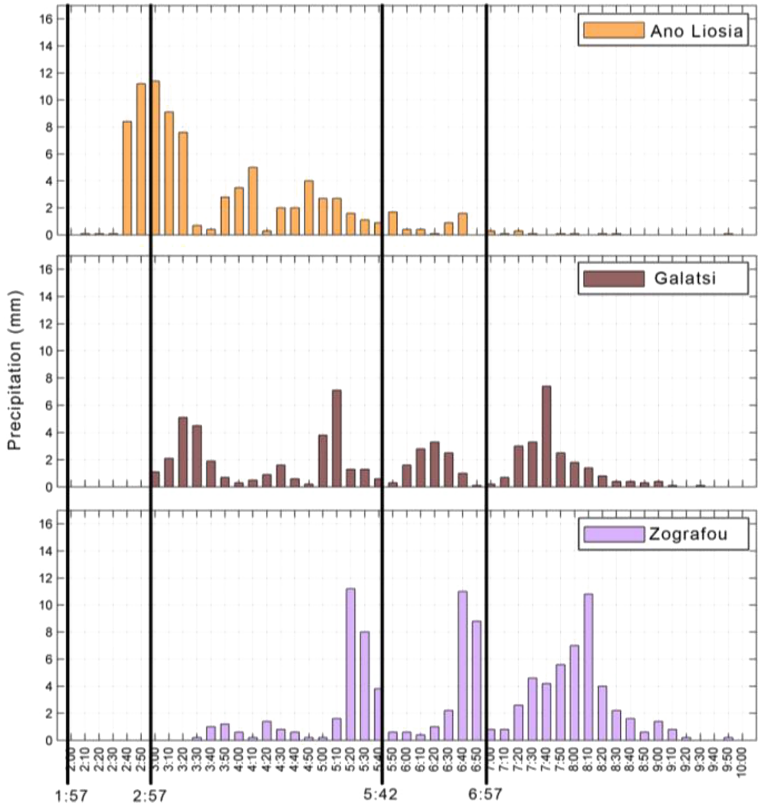

Figure 12. Precipitation data every ten minutes at three stations Ano Liosia, Galatsi and Zografou.

NHESSD
3, 2191–2219, 2015

An assessment of the potential of earth observation data to detect storm cells

T. Mavrakou and C. Cartalis